AGU PUBLICATIONS

Geophysical Research Letters

RESEARCH LETTER

10.1002/2016GL069676

Key Points:
- Rapid ocean warming, as during the PETM, can lead to rapid hydrate dissociation, but methane release to the ocean is delayed and gradual
- In our models, most of the methane released from hydrate remains in the sediment pores, with only a small fraction reaching the ocean
- A late Paleocene hydrate inventory of at least 4000 Pg is needed to explain the PETM carbon isotope excursion

Supporting Information:
- Supporting Information S1

Correspondence to:
T. A. Minshull,
tmin@noc.soton.ac.uk

Citation:
Minshull, T. A., H. Marín-Moreno, D. I. Armstrong McKay, and P. A. Wilson (2016), Mechanistic insights into a hydrate contribution to the Paleocene-Eocene carbon cycle perturbation from coupled thermohydraulic simulations, *Geophys. Res. Lett.*, *43*, 8637–8644, doi:10.1002/2016GL069676.

Received 17 MAR 2016
Accepted 28 JUL 2016
Accepted article online 29 JUL 2016
Published online 30 AUG 2016

Mechanistic insights into a hydrate contribution to the Paleocene-Eocene carbon cycle perturbation from coupled thermohydraulic simulations

T. A. Minshull[1], H. Marín-Moreno[2,3], D. I. Armstrong McKay[1,4], and P. A. Wilson[1]

[1]National Oceanography Centre Southampton, University of Southampton, Southampton, UK, [2]Istituto Nazionale di Oceanografia e di Geofisica Sperimentale, Trieste, Italy, [3]National Oceanography Centre, Southampton, UK, [4]Geography and Environment, University of Southampton, Southampton, UK

Abstract During the Paleocene-Eocene Thermal Maximum (PETM), the carbon isotopic signature ($\delta^{13}C$) of surface carbon-bearing phases decreased abruptly by at least 2.5 to 3.0‰. This carbon isotope excursion (CIE) has been attributed to widespread methane hydrate dissociation in response to rapid ocean warming. We ran a thermohydraulic modeling code to simulate hydrate dissociation due to ocean warming for various PETM scenarios. Our results show that hydrate dissociation in response to such warming can be rapid but suggest that methane release to the ocean is modest and delayed by hundreds to thousands of years after the onset of dissociation, limiting the potential for positive feedback from emission-induced warming. In all of our simulations at least half of the dissociated hydrate methane remains beneath the seabed, suggesting that the pre-PETM hydrate inventory needed to account for all of the CIE is at least double that required for isotopic mass balance.

1. Introduction

Methane is a strong greenhouse gas that oxidizes in about a decade to carbon dioxide and can thereby continue to impact climate for many millennia [*Archer and Brovkin*, 2008]. Methane hydrates are stable at high pressures and low temperatures and can accumulate beneath the deep ocean over millions of years. If the overlying ocean warms, hydrate that has accumulated beneath the seabed over a long period can dissociate and methane may be released into the ocean. Present-day venting into the oceans at several locations may be attributed to such a mechanism [*Darnell and Flemings*, 2015; *Phrampus and Hornbach*, 2012; *Phrampus et al.*, 2014; *Westbrook et al.*, 2009], although the origin of the methane involved remains controversial [*Berndt et al.*, 2014]. Widespread hydrate dissociation has the potential to lead to a positive feedback in which the released methane and its oxidation product, carbon dioxide, enhance warming [*Archer and Buffett*, 2005]. On the centennial to millennial time scales over which this feedback is hypothesized to operate, however, several processes below the seafloor have the potential to slow, shut down, or even reverse methane release in response to thermal dissociation of gas hydrate. In addition to the long-recognized effects on heat propagation of thermal diffusion [e.g., *Dickens et al.*, 1995], it is important to consider the role of latent heat in hydrate dissociation [e.g., *Thatcher et al.*, 2013], and the effects of bubble transport and biogeochemical consumption [e.g., *Boetius and Wenzhöfer*, 2013] on methane release from the seabed.

The early Paleogene was characterized by several "hyperthermals," which appear to represent geologically brief (<200 kyr) episodes of global warming and massive carbon input associated with decreases in the stable oxygen and carbon isotope composition of biogenic carbonate [*Littler et al.*, 2014; *Sexton et al.*, 2011; *Zachos et al.*, 2008]. The most extreme and the best studied of these events, the Paleocene-Eocene Thermal Maximum (PETM; Figure 1), is characterized by an increase in the global mean surface ocean temperature of ~5°C, warming of the surface ocean locally by up to 9°C, shoaling of the depth in the ocean of total carbonate dissolution in seafloor sediments by at least 2 km in the Atlantic, the extinction of many species of benthic foraminifera, and a prominent carbon isotopic excursion (CIE) involving a decrease in $\delta^{13}C$ of carbon-bearing phases by at least 2.5–3.0‰ [*Dickens*, 2011; *Dunkley Jones et al.*, 2013; *Foster et al.*, 2013; *Zachos et al.*, 2005; *Zeebe et al.*, 2009]. These observations indicate rapid perturbation of the exogenic carbon cycle through the release of buried organic carbon.

Mass balance considerations suggest that between 2000 and 13,000 Pg of carbon rich in the ^{12}C isotope must have been released in less than 10,000 years at the start of this event [*Cui et al.*, 2011; *Dickens*, 2011;

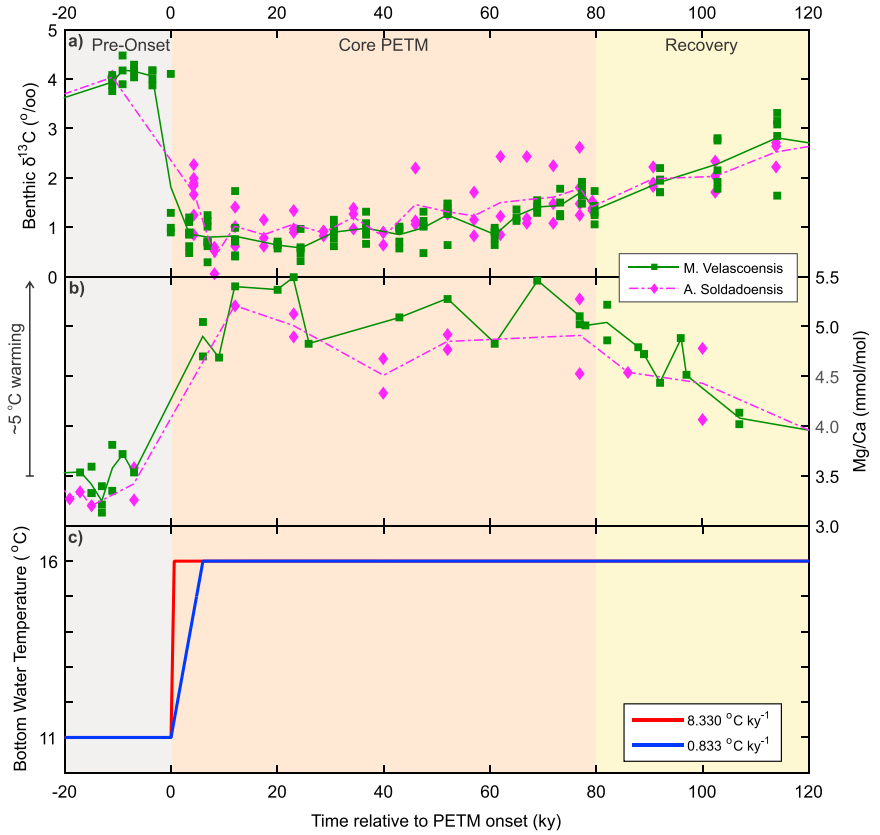

Figure 1. Abrupt warming and carbon cycle perturbation across the PETM revealed in (a) $\delta^{13}C$ [*Zachos et al.*, 2003; with age model of *Penman et al.*, 2014] and (b) Mg/Ca [*Penman et al.*, 2014] data from planktic foraminifera (*Morozovella velascoensis*: green squares and solid line for average, and *Acaranina soldadoensis*: magenta diamonds and dot-dashed line for average) from ODP Site 1209 (North Pacific) revealing an ~3‰ carbon isotope excursion and an ~5°C warming, respectively. (c) The two bottom water temperature functions (a 5°C increase over either 0.6 kyr (8.330°C kyr^{-1}) or 6 kyr (0.8330°C kyr^{-1})) used in this study. The grey shading indicates the pre-PETM baseline, orange shading the core of the PETM, and yellow shading the post-PETM recovery.

Dickens et al., 1995; *Panchuk et al.*, 2008; *Zeebe et al.*, 2009]. Most current estimates for the duration of the initial isotope excursion are in the range of 1 to 10 kyr; the bimodal isotope distribution seen in records from individual shells in expanded sections point to the short end member of this range [*Zachos et al.*, 2007], but there is little support for a much shorter (decadal) perturbation [*Wright and Schaller*, 2013]. As a result, the PETM has been proposed as a partial analogue to current anthropogenic emissions and climate change, where the total mass of carbon input is comparable but where anthropogenic rates of carbon emission are an order of magnitude faster [*Zeebe et al.*, 2016]. Several sources of carbon have been hypothesized to be involved including permafrost or kerogen and volcanism-induced thermogenic methane during the emplacement of the North Atlantic Volcanic Province [*Cui et al.*, 2011; *DeConto et al.*, 2012; *Svensen et al.*, 2004], but the longest-standing hypothesized mechanism involves widespread dissociation of methane hydrates [*Dickens*, 2011; *Dickens et al.*, 1995; *Sluijs et al.*, 2007; *Thomas et al.*, 2002].

Because PETM modeling efforts to date have been motivated largely by a need to understand the basic mass balance [*Dickens*, 2011] they have, understandably, employed relatively simplistic numerical analysis. Commonly, for example, it is assumed that the time scale for methane release is primarily controlled by the diffusion of heat into the subsurface [e.g., *Katz et al.*, 2001] and that all the methane from hydrate dissociation rises rapidly to the seabed. *Xu et al.* [2001] developed a model for the PETM that explicitly considers fluid flow and methane transport. However, that model (i) does not account for the effects of latent heat, which slows the downward propagation of heat [*Thatcher et al.*, 2013] or for salinity variations that perturb the phase boundary; (ii) only considers methane transport in solution, without bubbles; and (iii) assumes high

fluid flow rates more representative of active than passive margins. Thus, enhanced methane transport into the ocean results primarily from increased methane solubility in warmer pore fluids. A more recent simulation of the PETM incorporates the effects of latent heat but not the effects of pressure and salinity variations resulting from hydrate dissociation [*Zeebe*, 2013]. That simulation assumes that upon dissociation, methane is rapidly released into the ocean and therefore does not consider the physical and biogeochemical processes that may slow its ascent and perhaps even prevent its arrival at the seafloor. Here we employ a more sophisticated numerical model of subseabed processes that was developed to understand present-day methane release and to predict future release [*Marín-Moreno et al*., 2013; *Reagan and Moridis*, 2007; *Stranne et al*., 2016; *Thatcher et al*., 2013]. We simulate the response of hypothetical slope sediment sequences representative of those likely to have contained methane hydrate during the Paleocene to some simple PETM warming scenarios to show how methane transport and dissolution processes influence the time scale and magnitude of methane generation and release into the ocean.

2. Method and Results

We ran one-dimensional simulations using the thermohydraulic fully coupled TOUGH+HYDRATE code [*Moridis et al*., 2012]. This code numerically solves coupled equations of heat and mass balance and hence can model the nonisothermal gas release, phase behavior, and flow of fluids and heat in gas hydrate-bearing geological systems. The continuum balance equations of each of the mass components (water, methane, and salt) and heat are discretized in space by the integral finite difference method [e.g., *Narasimhan and Witherspoon*, 1976] and in time by first-order finite difference. The resultant set of coupled, nonlinear, algebraic equations are solved by Newton-Raphson iteration, approximating the Jacobian matrix by numerical differentiation and using sparse direct matrix methods or iteratively with a preconditioned conjugate gradient method [*Moridis and Pruess*, 1995]. We assumed equilibrium conditions for hydrate formation and dissociation and that the mass components water, methane, and salt were partitioned between four possible phases: hydrate (water and methane), aqueous (water, methane, and salt), gas (water and methane), and ice (water). We modeled heat exchanges due to conduction, convection, hydrate formation and dissociation, and methane and salt dissolution. We used Darcy's law for the flow of water and methane in the aqueous and gas phases, respectively, and for the advective transport of methane and salt in the aqueous phase. For the molecular diffusive transport of methane and salt within the aqueous phase we used a Fick-type law. Calculated seabed methane emissions include contributions from both methane bubble flow and dissolved methane. TOUGH+HYDRATE is a well-documented code and has been employed in several works to model warming-induced hydrate dissociation [e.g., *Marín-Moreno et al*., 2013; *Reagan and Moridis*, 2007; *Stranne et al*., 2016; *Thatcher et al*., 2013]. However, for completeness, further details of this code and our approach to its use are given in the supporting information.

Our models used parameters matching those of *Zeebe* [2013] and *Marín-Moreno et al*. [2013] (supporting information). Model sensitivity to a wide range of parameters has been explored previously [*Marín-Moreno et al*., 2013; *Thatcher et al*., 2013]. The permeability and the irreducible gas saturation (IGS), above which free gas can flow, are key parameters controlling the onset of methane emissions and amount emitted. If permeabilities appropriate to hemipelagic sediments are used, hydrate dissociation leads to a buildup of pore pressure that would be sufficient to fracture such sediments [*Stranne et al*., 2016; *Thatcher et al*., 2013]. The released version of TOUGH+HYDRATE can neither simulate the formation of fractures nor, in a one-dimensional model, account for preexisting fractures. The formation of fractures has been tackled recently by *Marín-Moreno et al*. [2015a] and *Stranne et al*. [2016] using an a posteriori off-line approach, following *Daigle and Dugan*'s [2010] normalized overpressure ratio criterion. Here we model porous flow in pristine hemipelagic sediments using an intrinsic permeability of 10^{-16} m^2 and approximate fracture flow by modeling porous flow with an enhanced intrinsic permeability of 10^{-13} m^2 (supporting information). Our simulations compute the evolution of intrinsic permeability with porosity according to *Xu et al*.'s [2004] relationship, the methane and water relative permeabilities according to a modified version of *Stone*'s [1970] first three-phase relative permeability method, the capillary pressure according to *van Genuchten*'s [1980] law, and the bulk thermal conductivity of the sediments according to *Moridis et al*. [2005] (supporting information). The relative permeability and capillary pressure models were initially developed for partially saturated sediments, but they can also be used to model fluid flow in hydrate systems with minor modifications depending on hydrate saturation [*Dai and Santamarina*, 2013; *Dai and Seol*, 2014]. We use IGSs of 2%,

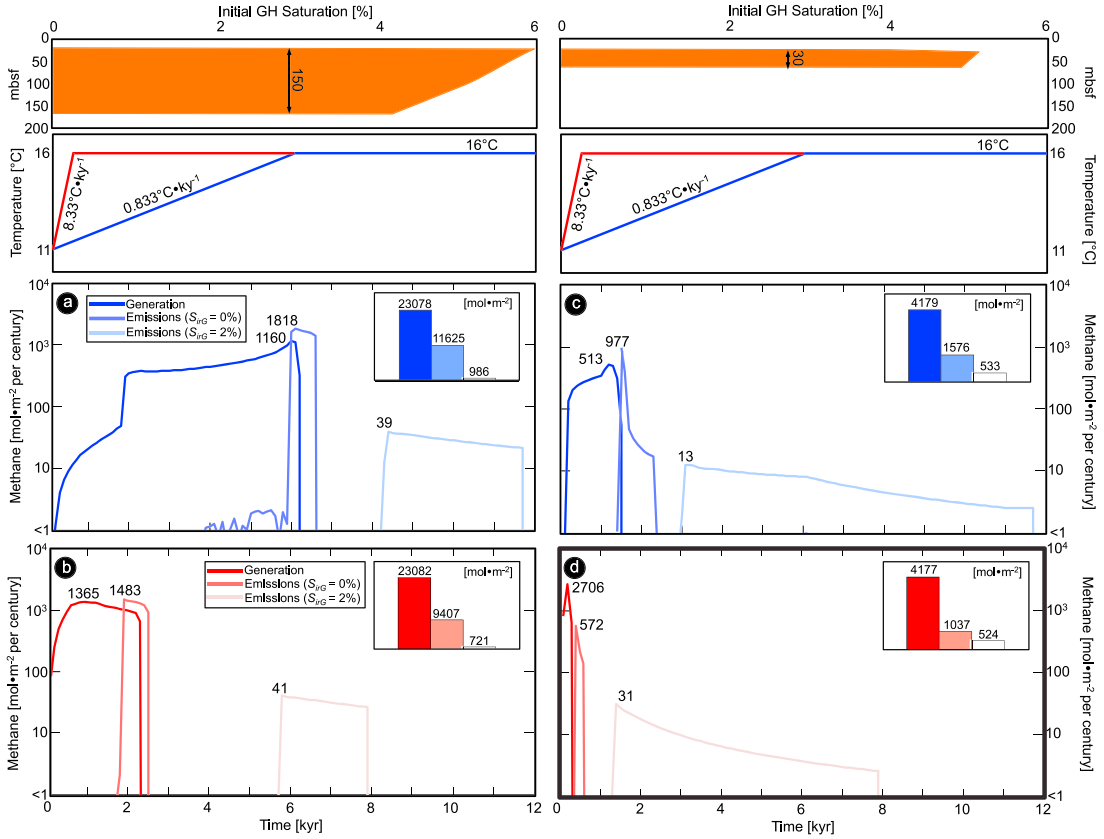

Figure 2. Methane generation from hydrate dissociation (thick lines) and associated seabed methane emissions for an intrinsic permeability of 10^{-13} m^2, irreducible gas saturations of 0% (medium lines) and 2% (pale lines), and for 0.833°C kyr^{-1} warming (blue) and 8.330°C kyr^{-1} warming (red). (a and b) Simulations with a 150 m thick hydrate layer and (c and d) simulations with a 30 m thick hydrate layer. Note that the vertical scale is logarithmic. The histograms show the total methane generation and emissions.

appropriate to porous flow in gas hydrate-bearing geologic systems [e.g., *Liu and Flemings*, 2007; *Thatcher et al*., 2013], and 0%, which may be appropriate for purely fracture flow. The anaerobic oxidation of methane in the sulfate reduction zone can consume between 10 and 20% (for high fluid flow rates) and 80% (for lower rates) of dissolved methane approaching the seabed [*Boetius and Wenzhöfer*, 2013]. We represented the effects of this process by including in our starting models a methane-free zone close to the seabed, in which methane approaching the seabed dissolves. This approach likely overestimates methane consumption at the base of the methane-free zone initially but perhaps underestimates methane consumption close to the seabed at later times, as methane concentrations build up. Following *Zeebe* [2013], we used a thickness of 20 m for the methane-free zone.

We assumed an initial hydrate saturation of ~5% between the methane-free zone and the hydrate stability limit, which is representative of estimated saturations beneath the modern ocean [e.g., *Milkov*, 2004; *Thatcher et al*., 2013]. We used a similar seabed temperature function to that of *Zeebe* [2013] but considered only his initial temperature rise of 5°C at the PETM onset, with an initial deep ocean temperature of 11°C. Following this initial temperature rise, we maintained the seabed temperature at a constant value until the end of the model runs after 20 kyr (Figure 1). We considered two alternative durations for the initial temperature rise: 6 kyr, as used by *Zeebe* [2013], and 0.6 kyr, to explore the effect of a very short duration end-member. To capture the range of possible behaviors, we also ran models for two different water depths: 1750 m, where the hydrate stability zone (HSZ) is thick (~150 m) and hydrate remains stable at the seabed at maximum PETM temperatures, and 1100 m, where the hydrate stability zone is thin (~30 m) and hydrate is stable at the seabed before warming begins but becomes unstable during the initial PETM temperature rise (Figure 2). We imposed a basal heat flow of 56 mW m^{-2} to obtain initial thicknesses of the gas hydrate stability zone that match those of *Zeebe* [2013].

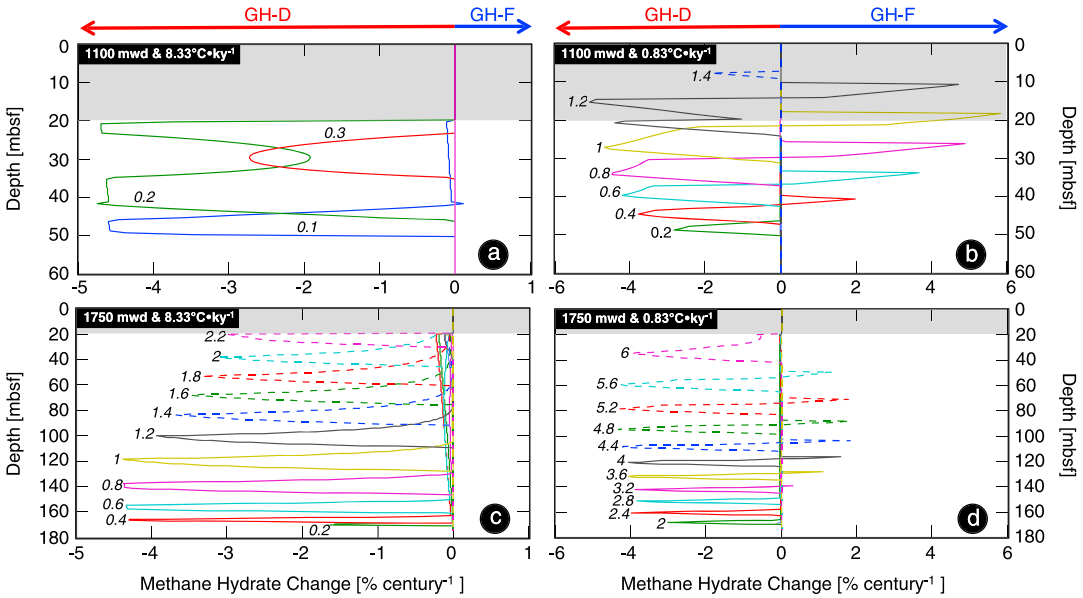

Figure 3. Rate of hydrate dissociation and/or dissolution (GH-D) and hydrate formation (GH-F) at different times (indicated by the values in kiloyear next to each line), for models with an intrinsic permeability of 10^{-13} m^2 and irreducible gas saturation of 2%. Results for a 30 m hydrate layer for a warming rate of (a) 8.33°C kyr^{-1} and (b) 0.833°C kyr^{-1}. (c and d) The equivalent plots for a 150 m hydrate layer. In Figures 3a and 3c, the relatively sharp peaks represent the dissociation, while the parts of the curves with negative values that slowly increase toward the seabed represent the dissolution.

At 1750 m water depth (mwd) hydrate dissociation peaks ~1 kyr and 6 kyr after the initial temperature rise, for 0.6 kyr and 6 kyr warming periods, respectively, before dropping to zero as the hydrate is exhausted. At 1100 mwd these peaks are 0.2 and 1.2 kyr after the initial warming. For a 0.6 kyr warming period, hydrate dissolution due to increased methane solubility at higher temperatures [*Waite et al.*, 2009] occurs initially throughout almost the entire HSZ and reaches a maximum at the top of the HSZ (Figures 3a and 3c). Hydrate dissociation occurs at the base of the HSZ and starts earlier for 1100 mwd because hydrate is present in a much thinner zone (Figures 3a and 3c). The dissociation rate is over an order of magnitude greater than the rate of hydrate dissolution (Figure 3c). With this very rapid warming and when the HSZ is thin, similar rates of hydrate dissociation can occur on the top and bottom of the HSZ with lower rates occurring in between (Figure 3a). This behavior may also occur in modern hydrate systems affected by ocean warming [*Marin-Moreno et al.*, 2015b]. For a warming period of 6 kyr, hydrate dissolution does not occur and dissociation starts at the base of the HSZ. This relatively slow warming rate allows hydrate reformation from the ascent of methane released by hydrate dissociation below (Figures 3b and 3d). Note that intrinsic permeability and IGS do not influence the rates of hydrate dissociation and dissolution and only influence the rate of hydrate reformation. Therefore, the results presented in Figure 3 are very similar to those obtained in the other cases modeled.

A striking result from our study is that in all cases, hydrate dissociation and methane generation in the sediment column are poorly related to methane release to the ocean, both in timing and in magnitude (Figure 2). The models with an intrinsic permeability of 10^{-16} m^2 show zero emissions over the 20 kyr duration of our runs. For the models with an intrinsic permeability of 10^{-13} m^2, gas escape into the ocean is delayed by 0.3–3 kyr and 2–8 kyr after gas is generated by hydrate dissociation, for the 1100 and 1750 mwd models, respectively. This delay results from the slow vertical rise of gas when it is close to the IGS and increases as the IGS increases (Figure 2). It decreases as intrinsic permeability increases but changes little for permeabilities greater than 10^{-13} m^2 [*Thatcher et al.*, 2013]. This result is important because the delay limits the potential for positive feedback between hydrate dissociation and climate change. For an IGS of 2%, methane release into the ocean is spread over a long period of time: 7–8 kyr for 1100 mwd and 3–4 kyr for 1750 mwd. The shorter duration at 1750 mwd, despite the thicker HSZ, occurs because a larger amount of released methane is present as free gas, which increases the relative permeability for gas and hence the rate

of methane ascent. If this saturation threshold is removed, the duration of flow is reduced to 300–800 years, and the variation with water depth is more complex. Importantly, at least half of the methane released by dissociation remains in solution or as gas bubbles beneath the seabed at the end of these model runs (Figure 2). Dissolution occurs within the initially methane-free sulfate reduction zone but also elsewhere because of the solubility increase due to warming. For an IGS of 2%, more methane remains beneath the seabed as gas bubbles below that threshold, and less than 15% of the dissociated methane escapes to the ocean (Figure 2).

3. Discussion and Conclusions

The delays in methane release associated with thermal diffusion to the seabed have been pointed out before [e.g., *Dickens et al*., 1995; *Zeebe*, 2013]. However, our analysis shows that there are additional mechanisms that both slow and reduce the methane release into the ocean. These mechanisms operate also in the modern ocean [*Stranne et al*., 2016]. The delays will be less and emissions will be more complete in shallower water, with higher geothermal gradient and with a thinner methane-free zone, and vice versa. The different responses of the different parts of the system will result in a net long slow rise in emissions followed by a long slow decline. More rapid escape to the ocean might be triggered by catastrophic slumping, but such events would need to occur globally over a millennial time scale to dominate the global flux into the ocean [*Nisbet et al*., 2009]. If such catastrophic mechanisms are excluded, and our model runs are broadly representative, then the CIE can be explained by hydrate dissociation only if (i) fractures were present or formed during hydrate dissociation to enhance the permeability and (ii) the minimum hydrate inventory is at least double the approximately 2000 Pg C [e.g., *Dickens et al*., 1995] required to account for the CIE based on isotopic mass balance considerations. Given a warm Paleocene ocean and therefore a more restricted hydrate stability field than at present, such a large hydrate inventory is difficult to reconcile with model-based estimates of the modern inventory of approximately 550–3000 Pg C [*Buffett and Archer*, 2004; *Kretschmer et al*., 2015; *Piñero et al*., 2013; *Yamamoto et al*., 2014]. These inventories might be reconciled if the modern inventory is underestimated by models [*Beaudoin et al*., 2014] and/or if higher seabed temperatures stimulated significantly greater methanogenesis in the late Paleocene than today [*Gu et al*., 2011].

We conclude the following:

1. Rapid warming of the deep ocean, such as during the PETM, can lead to rapid hydrate dissociation, but methane release to the ocean is delayed significantly by transport processes through the hydrate stability field.
2. In our models, most of the methane released from hydrate remains in the sediment pores, as dissolved methane or as free gas and only a small fraction reaches the ocean.
3. To explain the global carbon isotopic excursion at the PETM onset, the global hydrate inventory needs to be significantly larger than that required for isotopic mass balance and the permeability of the sediments needs to be enhanced by fractures.
4. Global PETM warming may well have resulted in hydrate dissociation and release of methane to the global ocean, but our results raise further challenges around the mechanism of these processes.

Acknowledgments
We thank Gerald Dickens and an anonymous reviewer for their thoughtful comments that considerably improved the quality of the manuscript. T.A.M. and P.A.W. were supported by Royal Society Wolfson Research Merit awards. H.M.M. was partly supported by the TALENTS FVG Programme—Activity 1—Incoming mobility scheme—European Social Fund, Operational Programme 2007–2013, Objective 2 Regional Competitiveness and Employment, Axis 5 Transnational cooperation. D.I.A.M. was supported by a Natural Environment Research Council PhD studentship (NERC grant NE/J500112/1). The data used in this paper are published in the cited sources, and the code used is available via http://esd1.lbl.gov/research/projects/tough/software/.

References

Archer, D., and B. Buffett (2005), Time-dependent response of the global ocean clathrate reservoir to climatic and anthropogenic forcing, *Geochem. Geophys. Geosyst.*, *6*, Q03002, doi:10.1029/2004GC000854.

Archer, D., and V. Brovkin (2008), The millennial atmospheric lifetime of anthropogenic CO_2, *Clim. Change*, *90*(3), 283–297.

Beaudoin, Y. C., W. Waite, R. Boswell, and S. R. Dallimore (Eds.) (2014), *Frozen Heat: A UNEP Global Outlook on Methane Gas Hydrates*, vol. 1, 77 pp., United Nations Environmental Programme, GRID-Arendal, Norway.

Berndt, C., et al. (2014), Temporal constraints on hydrate-controlled methane seepage off Svalbard, *Science*, *343*(6168), 284–287.

Boetius, A., and F. Wenzhöfer (2013), Seafloor oxygen consumption fuelled by methane from cold seeps, *Nat. Geosci.*, *6*(9), 725–734.

Buffett, B., and D. Archer (2004), Global inventory of methane clathrate: Sensitivity to changes in the deep ocean, *Earth Planet. Sci. Lett.*, *227*(3), 185–199.

Cui, Y., L. R. Kump, A. J. Ridgwell, A. J. Charles, C. K. Junium, A. F. Diefendorf, K. H. Freeman, N. M. Urban, and I. C. Harding (2011), Slow release of fossil carbon during the Palaeocene-Eocene Thermal Maximum, *Nat. Geosci.*, *4*(7), 481–485.

Dai, S., and J. C. Santamarina (2013), Water retention curve for hydrate-bearing sediments, *Geophys. Res. Lett.*, *40*, 5637–5641, doi:10.1002/2013GL057884.

Dai, S., and Y. Seol (2014), Water permeability in hydrate-bearing sediments: A pore-scale study, *Geophys. Res. Lett.*, *41*, 4176–4184, doi:10.1002/2014GL060535.

Daigle, H., and B. Dugan (2010), Origin and evolution of fracture-hosted methane hydrate deposits, *J. Geophys. Res.*, *115*, B11103, doi:10.1029/2010JB007492.
Darnell, K. N., and P. B. Flemings (2015), Transient seafloor venting on continental slopes from warming-induced methane hydrate dissociation, *Geophys. Res. Lett.*, *42*, 10,765–10,772, doi:10.1002/2015GL067012.
DeConto, R. M., S. Galeotti, M. Pagani, D. Tracy, K. Schaefer, T. Zhang, D. Pollard, and D. J. Beerling (2012), Past extreme warming events linked to massive carbon release from thawing permafrost, *Nature*, *484*(7392), 87–91.
Dickens, G. R. (2011), Down the Rabbit Hole: Toward appropriate discussion of methane release from gas hydrate systems during the Paleocene-Eocene Thermal Maximum and other past hyperthermal events, *Clim. Past*, *7*(3), 831–846.
Dickens, G. R., J. R. O'Neil, D. K. Rea, and R. M. Owen (1995), Dissociation of oceanic methane hydrate as a cause of the carbon isotope excursion at the end of the Paleocene, *Paleoceanography*, *10*(6), 965–971, doi:10.1029/95PA02087.
Dunkley Jones, T., D. J. Lunt, D. N. Schmidt, A. Ridgwell, A. Sluijs, P. J. Valdes, and M. Maslin (2013), Climate model and proxy data constraints on ocean warming across the Paleocene-Eocene Thermal Maximum, *Earth Sci. Rev.*, *125*, 123–145.
Foster, L. C., D. N. Schmidt, E. Thomas, S. Arndt, and A. Ridgwell (2013), Surviving rapid climate change in the deep sea during the Paleogene hyperthermals, *Proc. Natl. Acad. Sci. U.S.A.*, *110*(23), 9273–9276.
Gu, G. S., G. R. Dickens, G. Bhatnagar, F. S. Colwell, G. J. Hirasaki, and W. G. Chapman (2011), Abundant early Palaeogene marine gas hydrates despite warm deep-ocean temperatures, *Nat. Geosci.*, *4*(12), 848–851.
Katz, M. E., B. S. Cramer, G. S. Mountain, S. Katz, and K. G. Miller (2001), Uncorking the bottle: What triggered the Paleocene/Eocene Thermal Maximum methane release?, *Paleoceanography*, *16*(6), 549–562, doi:10.1029/2000PA000615.
Kretschmer, K., A. Biastoch, L. Rüpke, and E. Burwicz (2015), Modeling the fate of methane hydrates under global warming, *Global Biogeochem. Cycles*, *29*, 610–625, doi:10.1002/2014GB005011.
Littler, K., U. Röhl, T. Westerhold, and J. C. Zachos (2014), A high-resolution benthic stable-isotope record for the South Atlantic: Implications for orbital-scale changes in late Paleocene, early Eocene climate and carbon cycling, *Earth Planet. Sci. Lett.*, *401*, 18–30.
Liu, X., and P. B. Flemings (2007), Dynamic multiphase flow model of hydrate formation in marine sediments, *J. Geophys. Res.*, *112*, B03101, doi:10.1029/2005JB004227.
Marín-Moreno, H., T. A. Minshull, G. K. Westbrook, B. Sinha, and S. Sarkar (2013), The response of methane hydrate beneath the seabed offshore Svalbard to ocean warming during the next three centuries, *Geophys. Res. Lett.*, *40*, 5159–5163, doi:10.1002/grl.50985.
Marín-Moreno, H., M. Giustiniani, and U. Tinivella (2015a), The potential response of the hydrate reservoir in the South Shetland Margin, Antarctic Peninsula, to ocean warming over the 21st century, *Polar Res.*, *34*, 27,443, doi:10.3402/polar.v34.27443.
Marin-Moreno, H., T. A. Minshull, G. K. Westbrook, and B. Sinha (2015b), Estimates of future warming-induced methane emissions from hydrate offshore West Svalbard for a range of climate models, *Geochem. Geophys. Geosyst.*, *16*, 1307–1323, doi:10.1002/2015GC005737.
Milkov, A. V. (2004), Global estimates of hydrate-bound gas in marine sediments: How much is really out there?, *Earth Sci. Rev.*, *66*(3), 183–197.
Moridis, G. J., Y. Seol, and T. Kneafsey (2005), Studies of reaction kinetics of methane hydrate dissociation in porous media, in *Proceedings of the 5th International Conference on Gas Hydrates*, vol. 1, pp. 21–30, Tapir Academic Press, Trondheim, Norway.
Moridis, G. J., M. B. Kowalsky, and K. Pruess (2012), TOUGH+HYDRATE v1.2 user's manual: A code for the simulation of system behaviour in hydrate-bearing geological media, Per. LBNL-0149E, Lawrence Berkeley Natl. Lab., Berkeley, Calif.
Moridis, G., and K. Pruess (1995), Flow and transport simulations using T2CG1, a package of conjugate gradient solvers for the TOUGH2 family of codes, Lawrence Berkeley Laboratory Report LBL-36235, Berkeley, Calif.
Narasimhan, T. N., and P. A. Witherspoon (1976), An integrated finite difference method for analyzing fluid flow in porous media, *Water Resour Res*, *12*(1), 57–64, doi:10.1029/WR012i001p00057.
Nisbet, E. G., S. M. Jones, J. Maclennan, G. Eagles, J. Moed, N. Warwick, S. Bekki, P. Braesicke, J. A. Pyle, and C. M. R. Fowler (2009), Kick-starting ancient warming, *Nat. Geosci.*, *2*(3), 156–159.
Panchuk, K., A. Ridgwell, and L. R. Kump (2008), Sedimentary response to Paleocene-Eocene Thermal Maximum carbon release: A model-data comparison, *Geology*, *36*(4), 315–318.
Penman, D. E., B. Hönisch, R. E. Zeebe, E. Thomas, and J. C. Zachos (2014), Rapid and sustained surface ocean acidification during the Paleocene-Eocene Thermal Maximum, *Paleoceanography*, *29*, 357–369, doi:10.1002/2014PA002621.
Phrampus, B. J., and M. J. Hornbach (2012), Recent changes to the Gulf Stream causing widespread gas hydrate destabilization, *Nature*, *490*(7421), 527–530.
Phrampus, B. J., M. J. Hornbach, C. D. Ruppel, and P. E. Hart (2014), Widespread gas hydrate instability on the upper U.S. Beaufort margin, *J. Geophys. Res. Solid Earth*, *119*, 8594–8609, doi:10.1002/2014JB011290.
Piñero, E., M. Marquardt, C. Hensen, M. Haeckel, and K. Wallmann (2013), Estimation of the global inventory of methane hydrates in marine sediments using transfer functions, *Biogeosciences*, *10*(2), 959–975.
Reagan, M. T., and G. J. Moridis (2007), Oceanic gas hydrate instability and dissociation under climate change scenarios, *Geophys. Res. Lett.*, *34*, L22709, doi:10.1029/2007GL031671.
Sexton, P. F., R. D. Norris, P. A. Wilson, H. Palike, T. Westerhold, U. Rohl, C. T. Bolton, and S. Gibbs (2011), Eocene global warming events driven by ventilation of oceanic dissolved organic carbon, *Nature*, *471*(7338), 349–52.
Sluijs, A., H. Brinkhuis, S. Schouten, S. M. Bohaty, C. M. John, J. C. Zachos, G.-J. Reichart, J. S. Sinninghe Damste, E. M. Crouch, and G. R. Dickens (2007), Environmental precursors to rapid light carbon injection at the Palaeocene/Eocene boundary, *Nature*, *450*(7173), 1218–1221.
Stone, H. (1970), Probability model for estimating three-phase relative permeability, *J. Pet. Technol.*, *22*(2), 214–218.
Stranne, C., M. O'Regan, G. R. Dickens, P. Crill, C. Miller, P. Preto, and M. Jakobsson (2016), Dynamic simulations of potential methane release from East Siberian continental slope sediments, *Geochem. Geophys. Geosyst.*, *17*, 872–886, doi:10.1002/2015GC006119.
Svensen, H., S. Planke, A. Malthe-Sorenssen, B. Jamtveit, R. Myklebust, T. Rasmussen Eidem, and S. S. Rey (2004), Release of methane from a volcanic basin as a mechanism for initial Eocene global warming, *Nature*, *429*(6991), 542–545.
Thatcher, K. E., G. K. Westbrook, S. Sarkar, and T. A. Minshull (2013), Methane release from warming-induced hydrate dissociation in the West Svalbard continental margin: Timing, rates, and geological controls, *J. Geophys. Res. Solid Earth*, *118*, 22–38, doi:10.1029/2012JB009605.
Thomas, D. J., J. C. Zachos, T. J. Bralower, E. Thomas, and S. Bohaty (2002), Warming the fuel for the fire: Evidence for the thermal dissociation of methane hydrate during the Paleocene-Eocene Thermal Maximum, *Geology*, *30*(12), 1067–1070.
Van Genuchten, M. T. (1980), A closed-form equation for predicting the hydraulic conductivity of unsaturated soils, *Soil Sci. Soc. Am. J.*, *44*(5), 892–898.
Waite, W. F., et al. (2009), Physical properties of hydrate-bearing sediments, *Rev. Geophys.*, *47*, RG4003, doi:10.1029/2008RG000279.
Westbrook, G. K., K. E. Thatcher, E. J. Rohling, A. M. Piotrowski, H. Palike, A. H. Osborne, E. G. Nisbet, T. A. Minshull, M. Lanoiselle, and R. H. James (2009), Escape of methane gas from the seabed along the West Spitsbergen continental margin, *Geophys. Res. Lett.*, *36*, L15608, doi:10.1029/2009GL039191.

Wright, J. D., and M. F. Schaller (2013), Evidence for a rapid release of carbon at the Paleocene-Eocene Thermal Maximum, *Proc. Natl. Acad. Sci. U.S.A.*, *110*(40), 15,908–15,913.

Xu, T., Y. Ontoy, P. Molling, N. Spycher, M. Parini, and K. Pruess (2004), Reactive transport modeling of injection well scaling and acidizing at Tiwi field, Philippines, *Geothermics*, *33*(4), 477–491.

Xu, W., R. P. Lowell, and E. T. Peltzer (2001), Effect of seafloor temperature and pressure variations on methane flux from a gas hydrate layer: Comparison between current and late Paleocene climate conditions, *J. Geophys. Res.*, *106*(B11), 26,413–26,423, doi:10.1029/2001JB000420.

Yamamoto, A., Y. Yamanaka, A. Oka, and A. Abe-Ouchi (2014), Ocean oxygen depletion due to decomposition of submarine methane hydrate, *Geophys. Res. Lett.*, *41*, 5075–5083, doi:10.1002/2014GL060483.

Zachos, J. C., M. W. Wara, S. Bohaty, M. L. Delaney, M. R. Petrizzo, A. Brill, T. J. Bralower, and I. Premoli-Silva (2003), A transient rise in tropical sea surface temperature during the Paleocene-Eocene Thermal Maximum, *Science*, *302*, 1551–1554.

Zachos, J. C., S. M. Bohaty, C. M. John, H. McCarren, D. C. Kelly, and T. Nielsen (2007), The Palaeocene-Eocene carbon isotope excursion: Constraints from individual shell planktonic foraminifer records, *Philos. Trans. R. Soc., A*, *365*(1856), 1829–1842.

Zachos, J. C., et al. (2005), Rapid acidification of the ocean during the Paleocene-Eocene Thermal Maximum, *Science*, *308*(5728), 1611–1615.

Zachos, J. C., G. R. Dickens, and R. E. Zeebe (2008), An early Cenozoic perspective on greenhouse warming and carbon-cycle dynamics, *Nature*, *451*(7176), 279–283.

Zeebe, R. E. (2013), What caused the long duration of the Paleocene-Eocene Thermal Maximum?, *Paleoceanography*, *28*, 440–452, doi:10.1002/palo.20039.

Zeebe, R. E., J. C. Zachos, and G. R. Dickens (2009), Carbon dioxide forcing alone insufficient to explain Palaeocene-Eocene Thermal Maximum warming, *Nat. Geosci.*, *2*(8), 576–580.

Zeebe, R. E., A. Ridgwell, and J. C. Zachos (2016), Anthropogenic carbon release rate unprecedented during the past 66 million years, *Nat. Geosci.*, *9*(4), 325–329.